AGU PUBLICATIONS

Water Resources Research

RESEARCH ARTICLE

10.1002/2014WR016245

Key Points:
- Calibration of the measured EMI data using direct ground truth measurements
- Inversion of multiconfiguration EMI data to infer distribution of soil salinity
- In situ measurements confirm spatial distribution of soil salinity

Correspondence to:
K. Z. Jadoon,
khan.jadoon@kaust.edu.sa

Citation:
Jadoon, K. Z., D. Moghadas, A. Jadoon, T. M. Missimer, S. K. Al-Mashharawi, and M. F. McCabe (2015), Estimation of soil salinity in a drip irrigation system by using joint inversion of multicoil electromagnetic induction measurements, *Water Resour. Res.*, *51*, 3490–3504, doi:10.1002/2014WR016245.

Received 5 AUG 2014
Accepted 6 MAR 2015
Accepted article online 13 MAR 2015
Published online 12 MAY 2015

Estimation of soil salinity in a drip irrigation system by using joint inversion of multicoil electromagnetic induction measurements

Khan Zaib Jadoon[1], Davood Moghadas[2], Aurangzeb Jadoon[1,3], Thomas M. Missimer[1,4], Samir K. Al-Mashharawi[1], and Matthew F. McCabe[1]

[1]Water Desalination and Reuse Center, King Abdullah University of Science and Technology, Thuwal, Saudi Arabia, [2]Federal Institute for Geosciences and Natural Resources (BGR), Hannover, Germany, [3]Department of Earth Sciences, COMSATS Institute of Information Technology, Abbottabad, Pakistan, [4]U. A. Whitaker College of Engineering, Florida Gulf Coast University, Fort Myers, Florida, USA

Abstract Low frequency electromagnetic induction (EMI) is becoming a useful tool for soil characterization due to its fast measurement capability and sensitivity to soil moisture and salinity. In this research, a new EMI system (the CMD mini-Explorer) is used for subsurface characterization of soil salinity in a drip irrigation system via a joint inversion approach of multiconfiguration EMI measurements. EMI measurements were conducted across a farm where Acacia trees are irrigated with brackish water. In situ measurements of vertical bulk electrical conductivity (σ_b) were recorded in different pits along one of the transects to calibrate the EMI measurements and to compare with the modeled electrical conductivity (σ) obtained by the joint inversion of multiconfiguration EMI measurements. Estimates of σ were then converted into the universal standard of soil salinity measurement (i.e., electrical conductivity of a saturated soil paste extract – EC_e). Soil apparent electrical conductivity (EC_a) was repeatedly measured with the CMD mini-Explorer to investigate the temperature stability of the new system at a fixed location, where the ambient air temperature increased from 26°C to 46°C. Results indicate that the new EMI system is very stable in high temperature environments, especially above 40°C, where most other approaches give unstable measurements. In addition, the distribution pattern of soil salinity is well estimated quantitatively by the joint inversion of multicomponent EMI measurements. The approach of joint inversion of EMI measurements allows for the quantitative mapping of the soil salinity distribution pattern and can be utilized for the management of soil salinity.

1. Introduction

In arid and semi-arid regions, soil salinity is a major issue due to its impact on agro-ecosystems, agricultural productivity and sustainability. High levels of soil salinity adversely affects plant growth and crop yield, soil and water quality, and can ultimately result in soil erosion and land degradation [*Allbed and Kumar*, 2013]. As a major environmental concern, it is essential to monitor and map soil salinity at an early stage to effectively use soil resources and maintain soil salinity levels below the salt tolerance of crops. To do this, the standard procedure to estimate the soil salinity of a soil sample is to measure the electrical conductivity of saturated soil paste extracts (i.e., EC_e) [*Bower and Wilcox*, 1965; *Rhoades et al*., 1999]. However, the EC_e method is time-consuming, labor intensive, subject to analyst error and/or experience in the preparation of the saturated paste, and is often costly for performing large-scale field inventories and monitoring. In this respect, geophysical methods such as electrical resistivity (ER) and low frequency electromagnetic induction (EMI) present as promising techniques to map the distribution of soil salinity at the field scale with a high spatial resolution [*Adamchuk et al*., 2004].

In the ER method, the Wenner electrode configuration has been successfully used for soil salinity assessment, in which four electrodes are equidistantly spaced in a straight line at the soil surface, with the two outer electrodes serving as the current and the two inner electrodes serving as the potential electrodes [*Rhoades et al*., 1999]. A number of investigations have compared ER and EMI systems over a range of agricultural settings. For instance, *Fritz et al*. [1999] and *Sudduth et al*. [2003] showed similarities in mapping patterns and high

correlation between collocated points (coefficient of correlation as high as 0.92). However, ER sensors require good contact between the soil and electrodes inserted into the subsurface and can therefore produce less reliable measurements in dry or stony soils [*Sudduth et al*., 2005]. *Corwin and Lesch* [2005a] noted that the use of EMI instruments has three advantages over the use of ER instruments, including: (1) the ability to take measurements on dry and stony soils, (2) the ability to traverse growing crops, and (3) the ability to traverse fields with beds and furrows. An additional advantage of the EMI sensor is that they can be used to characterize soil spatial variability across large areas, due to their higher operating speeds [*Abdu et al*., 2007].

In the last few decades, EMI techniques have been used increasingly to estimate soil salinity [*Lesch et al*., 1995; *Triantafilis et al*., 2000; *Corwin et al*., 2006; *Ganjegunte et al*., 2014]. EMI instruments measure the soil apparent electrical conductivity (EC_a), which represents a weighted average of the electrical conductivity distribution over a certain depth range. Measurements can be performed using two different coil orientations, defined as the horizontal coplanar loop (HCP) and vertical coplanar loop (VCP). Given the low induction number condition, *Mester et al*. [2011] showed that most information about the subsurface can be obtained by using different coil orientations, while different offsets have intermediate impact on the EMI response and changing frequencies (8–15 KHz) have a minor influence. Furthermore, the in-phase conductivity of the complex conductivity is frequency independent in the 1–100 kHz frequency range [*Borner*, 2006; *Revil*, 2012; *Revil et al*., 2014]. In nonsaline soils, EC_a variations are primarily a function of soil texture, moisture content, and cation exchange capacity [*Rhoades et al*., 1976; *Sudduth et al*., 2003]. However, in saline soil, the predominant mechanism causing the accumulation of salt in irrigated agricultural soils is loss of water through evaporation [*Ershadi et al*., 2014], leaving ever increasing concentrations of salt in the soil. Soil salinity is generally the soil property that dominates the EC_a measurement [*Corwin and Lesch*, 2005b]. An excellent review of the theoretical developments of EMI methods considering the near surface can be found in *Everett* [2012].

Numerous inversion approaches have been developed to obtain vertical variations of subsurface electrical conductivity using EMI systems [*Borchers et al*., 1997; *Santos*, 2004; *Jardani et al*., 2007; *Rudolph et al*., 2015]. For instance, *Li et al*. [2013] map the three-dimensional variation of soil salinity in a rice-paddy via the inversion of EC_a measured with the Geonics EM38 system. Due to the sensitivity of the instruments to calibration, one of the main limitations of the EMI technique is to obtain quantitative measurements of EC_a. A number of studies have also pointed out the lack of consistency of current methods to measure EC_a at the field scale [*Lavoue et al*., 2010; *Moghadas et al*., 2012]. However, obtaining precise EC_a values from EMI measurements is a prerequisite for inverse modeling. For decades, the lack of appropriate calibration methods hindered the development and application of quantitative EMI inversions. In addition, the inverse problem usually suffers from nonuniqueness issues and the inherent complexity of the objective function to optimize. To address this problem, *Minsley* [2011] used a 1-D electromagnetic model and proposed a trans-dimensional Bayesian Markov Chain Monte Carlo (MCMC) algorithm for model assessment and uncertainty analysis of frequency domain electromagnetic induction data.

In this paper, we performed joint-inversion of multi-offset, multi-orientation EMI measurements, collected using a CMD Mini-Explorer probe, to estimate the distribution pattern of soil salinity in a farm where Acacia trees were irrigated with brackish water via a drip irrigation system. We calibrated the measured EC_a using field information collected in situ and with capacitance sensors (i.e., 5TE Decagon probe). An electromagnetic forward model based on the full solution of the Maxwell's equation was used as the EMI measurements were collected under conditions of high induction number ($EC_a > 100$ mS/m). The sensitivity of the model with respect to the different retrieved parameters was investigated by utilizing the response surfaces of the objective function. Furthermore, a fixed point drift experiment was performed in field conditions to test the stability of the CMD-Mini explorer probe to temperature fluctuations. Finally, we related the modeled true electrical conductivity (σ) to soil salinity by establishing a relationship between bulk electrical conductivity (σ_b) measured by the capacitance sensor and the electrical conductivity of a saturated soil paste extract.

2. Methods and Experimental Setup

2.1. Electromagnetic Forward Model

There are two low frequency EMI forward models that can be employed to calculate apparent electrical conductivity from measured depth profile electrical conductivity. The most commonly used approach is the

local-sensitivity model introduced by *McNeill* [1980], which is based on the commutative response of the subsurface. This approach is valid under the low induction number condition. The second approach corresponds to the Maxwell-based full solution for the magnetic field measured over a horizontal layered medium given by *Keller and Frischknecht* [1966] and *Anderson* [1979]. Due to increased computational power, improved forward models based on the full solution of Maxwell's equation can be utilized [*Santos et al*., 2010]. In a low induction number condition the effective depth of exploration is independent of EC_a, whereas in high induction number condition the depth of exploration decreases with increasing EC_a [*Callegary et al*., 2007]. The electromagnetic forward model for a horizontal and vertical dipole source-receiver combination with an offset ρ over a multilayered earth can be written as:

$$EC_a^{HCP}(x,\rho)=\frac{-4\rho}{\omega\mu_0}\mathrm{Im}\left[\int_0^\infty R_0 J_0(\rho\lambda)\lambda^2 d\lambda\right] \tag{1}$$

$$EC_a^{VCP}(x,\rho)=\frac{-4}{\omega\mu_0}\mathrm{Im}\left[\int_0^\infty R_0 J_1(\rho\lambda)\lambda d\lambda\right] \tag{2}$$

In these expressions, EC_a^{HCP} and EC_a^{VCP}, correspond to apparent electrical conductivity measured in horizontal and vertical coplanar mode, J_0 and J_1 are the zero-order and first-order Bessel functions, λ is the radial wave number, μ_0 is permeability of the free space, ω is angular frequency and Im represents the quadrature component. The reflection factor R_0 is obtained recursively, beginning with the lowest layer N+1, where $R_{N+1}=0$:

$$R_n(h_n,\sigma_n)=\frac{\frac{\Gamma_n-\Gamma_{n+1}}{\Gamma_n+\Gamma_{n+1}}+R_{n+1}\exp\left(-2\Gamma_{n+1}h_{n+1}\right)}{1+\frac{\Gamma_n-\Gamma_{n+1}}{\Gamma_n+\Gamma_{n+1}}R_{n+1}\exp\left(-2\Gamma_{n+1}h_{n+1}\right)} \tag{3}$$

$$\Gamma_n=\sqrt{\lambda^2+\omega\mu_0 j\sigma_n} \tag{4}$$

and $\sigma_0=0$, h_n is the height, and σ_n is the electrical conductivity for the n^{th} layer. This formulation assumes that each layer is homogenous with infinite horizontal extent.

The electromagnetic forward model in not based on the low induction number assumption and returns more reliable apparent electrical conductivity values than the standard sensitivity curves of *McNeill* [1980]. EMI measurements were performed under high induction number conditions ($EC_a > 100$ mS/m) and as a result, the full solution of Maxwell's equation for electromagnetic forward modeling was utilized. *Lavoue et al*. [2010] and *Moghadas et al*. [2012] showed that the area below the effective depth range of EMI also contributes to the apparent electrical conductivity. As a result, for reference apparent electrical conductivity calculations (and also calibration) the whole measured conductivity data down to 1.5 m depth was considered. The electrical conductivity below this depth is equal to electrical conductivity of the last layer, which is assumed to be a homogeneous half-space.

2.2. Electromagnetic Induction System

The CMD Mini-Explorer was used to measure the EC_a in VCP and HCP orientations. Figure 1 shows a schematic of the CMD Mini-Explorer probe having a length of 1.28 m and a diameter of 0.05 m. The probe has to be rotated 90° to change the orientation from VCP to HCP mode. The CMD Mini-Explorer operates at 30 kHz frequency and has three receiver coils with 0.32, 0.71 and 1.18 m distances from the transmitter coil, referred to hereafter as ρ32, ρ71, and ρ118. The manufacturer indicates that the instrument has an effective depth range of 0.5, 1.0 and 1.8 m in the HCP mode, which is reduced to half (0.25, 0.5, and 0.9 m) by using the VCP orientation. As a consequence, EMI using this instrument returns six different apparent electrical conductivity values (utilizing three offsets with two coil orientations) with each corresponding to different depth ranges.

The CMD probe is used in conjunction with a handheld control unit, which is usually connected via bluetooth operating in the GHz band, which does not impact upon the 30 KHz operating frequency of the EMI sensor. The bluetooth connection allows for either a pedestrian hand-held survey or a GPS-enabled sled/cart mounted survey. The instrument can be setup efficiently within 3–5 min. An internal temperature compensation automatically provides absolute calibration of apparent conductivity data prior to each profile of data collected, which limits drift across the data set. The operational temperature of the instrument is

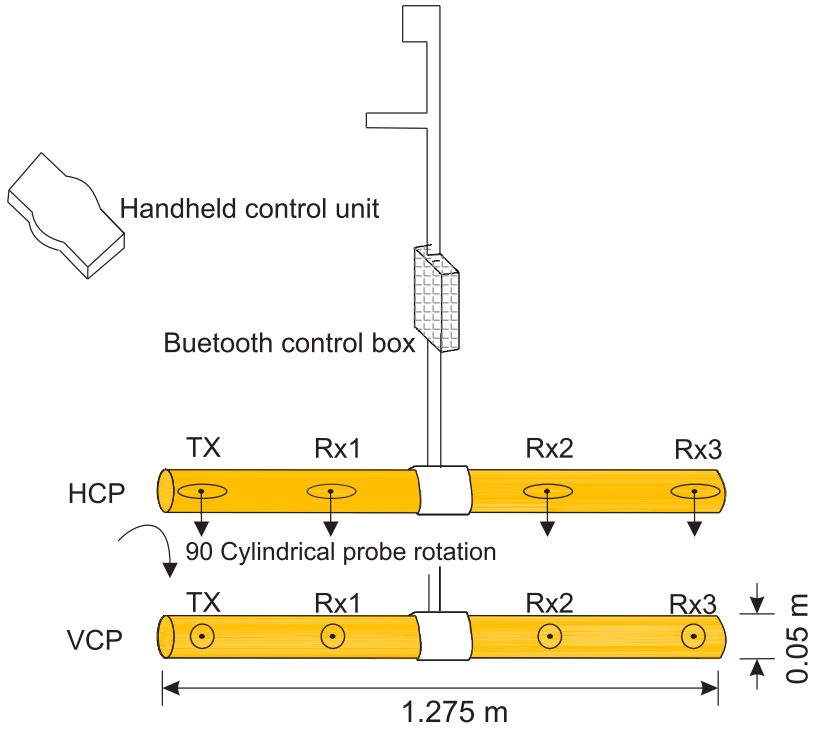

Figure 1. Schematic of coil geometry, configuration and orientation of the CMD Mini-Explorer (after *Bonsall et al*. [2013]). The three receiving coils R_{x1}, R_{x2} and R_{x3} are at a spacing of 0.32, 0.71 and 1.18 m from the transmitter coil, T_x. The system allows for measurements with both HCP and VCP orientations.

−10°C to +50°C and the temperature stability is ± 1 mS/m per 10°C change in temperature [*GF-Instruments*, 2011]. The weight of the CMD Mini-Explorer is 1.8 kg and can be held comfortably in one hand at the optimum probe height of approximately 0.05 m above the ground in order to ensure maximum depth of penetration. The probe height can be adjusted using a telescopic handle when encountering sites of variable terrain or vegetation cover.

2.3. Joint Inversion of Multiconfiguration EMI Data

Multiconfiguration EMI measurements contain different information on the subsurface. In the inversion, the subsurface is considered as a two layer problem and the parameter vector $\mathbf{b} = [\sigma_1, \sigma_2, h_1]$ is estimated by minimizing an objective function $\phi(\mathbf{b})$ defined as:

$$\phi(\mathbf{b}) = \frac{1}{N}\sum_{i=1}^{N}\left[\frac{|EC_{a,i}^{meas} - EC_{a,i}^{mod}|}{|EC_{a,i}^{meas}|}\right] \tag{5}$$

where N is the number of device configurations (six in our case), $EC_{a,i}^{meas}$ and $EC_{a,i}^{mod}$ are the measured and modeled soil apparent electrical conductivity, respectively. The objective function (Equation (5)) relates indirectly with the response function of the multilayered medium to its constitutive parameters. However, as in most electromagnetic inverse problems, this function is highly nonlinear and is characterized by oscillatory behavior and a multitude of local minima. The complex topography of the response surface demands the use of a robust global optimization algorithm. We combined sequentially the global multilevel coordinate search (GMCS) algorithm [*Huyer and Neumaier*, 1999] with the classical Nelder-Mead simplex algorithm (NMS) [*Lagarias et al*., 1998] to estimate the unknown parameters. A similar optimization approach has been used in other geophysical investigations [*Jadoon et al*., 2011; *Moghadas et al*., 2010]. The proposed inversion scheme is computationally inexpensive, as the electromagnetic forward model needs 0.12 s of computational time in MATLAB using a laptop with 2 GHz processor and 4 GB of RAM. It can be easily applied to field-scale EMI measurements and for large-scale multiconfiguration EMI measurements the code can also be parallelized [*von Hebel et al*., 2014].

The objective function in equation (5) was successfully used by *Mester et al*. [2011], who proposed a two step inversion approach to estimate the two-layer conductivity of a single transect by using multiconfiguration

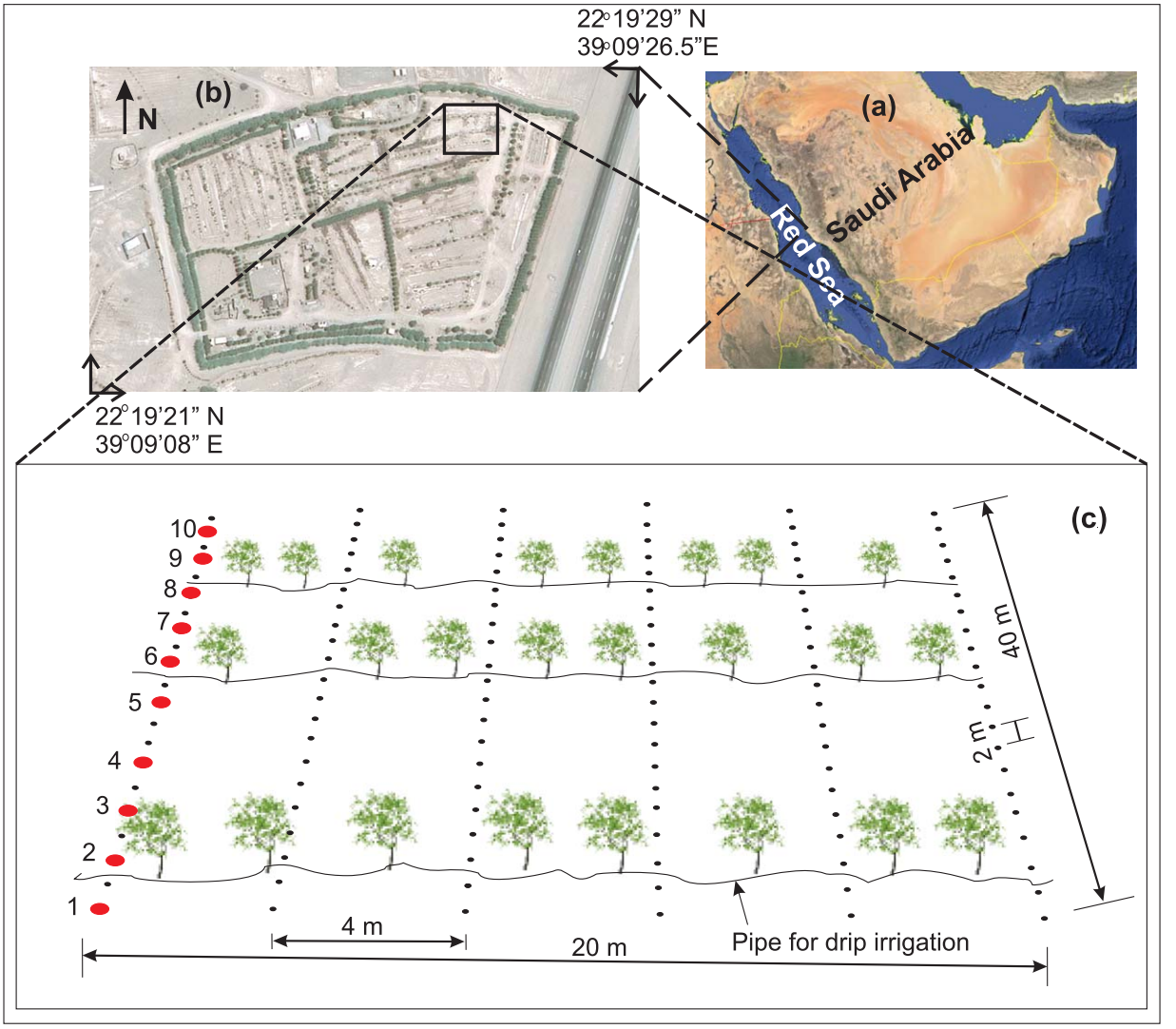

Figure 2. Geographical location of the study area: (a) aerial view of the farm where experiment was conducted, (b) the area where the EMI measurements were performed with, (c) the black and red dots represent the EMI measurement points and the pits with 1.5 m depth, respectively.

EMI measurements. In the first step, a global optimization algorithm was used to evaluate the misfit functions using a local-sensitivity model [*McNeill*, 1980], which is valid under the low induction number condition. In the second step, the parameters obtained through global optimization are used as a starting point for the local optimization, which is based on the simplex algorithm [*Lagarias et al.*, 1998] and uses the full solution of the Maxwell's equation as a forward model.

2.4. Experimental Setup

Measurements were conducted at a farm located at Al-Qadeimah, Makkah province, Saudi Arabia. The farm is at a distance of 6 km from the Red Sea coast. The site geology consists of late Tertiary sediments, predominantly sandy loam texture in nature, with a sand content of about 65 %. The top soil at the experimental site is a silty loam and has a silt content that increased from 50% in the top 30 cm layer to 55 % at a depth between 40 and 60 cm. The climate is hot and arid with an average annual temperature of 25°C and an annual rainfall of 55 mm.

Figures 2b and 2c depicts the areal view of the farm, densely surrounded by Acacia trees. Acacia, in general, is the most dominant tree in Saudi Arabia and elsewhere in the Arabian Peninsula [*Veseyfitzgerald*, 1957]. Acacia leaves and buds are rich in nitrogen and considered to be appropriate for animal feeding, especially

for goats and sheep. Most can grow in arid and semi-arid regions, with an average temperature of 40–50°C in summer. *Craig et al*. [1991] reported that Acacia is one of the most salt tolerant trees and can grow in soils having a mean EC_e 900–4160 mS/m in 0–60 cm depth. In arid and semi-arid regions, the high values of EC_a are mostly dominated by soil salinity as the salt accumulation in the soil occurs where potential evaporation exceeds irrigation and/or precipitation.

Figure 2c shows the area of investigation, with black dots representing the locations where EMI measurements were carried out at 2 m increments along a 40 m transect in a north-south direction. In total, six transects of EMI measurements were conducted to cover an area of 20 m by 40 m. The spacing between consecutive transects was kept constant at a 4 m interval. In the area of investigation, three rows of Acacia trees were irrigated with brackish water by using drip irrigation, with the measured electrical conductivity of the irrigation water (EC_w) being 4200 mS/m. Red circles in Figure 2c show the location of pits used to measure features of the vertical σ_b soil profile. Along this transect, 10 pits were dug to calibrate the drift in EMI measurement, with the vertical σ_b profile in each pit determined by using 5TE capacitance sensors (Decagon Devices, Pullman, USA) installed at 15 vertical locations within a depth range of 0.05–1.5 m depth. Operating at a frequency of 70 MHz, the 5TE sensor is able to measure soil moisture content, bulk electrical conductivity and temperature in almost any soil. EMI and 5TE measurements were performed 8 h after the drip irrigation system was stopped, so that the soil moisture should not be concentrated below the drippers and to give some time to reduce the soil moisture impact due to evaporation, root water uptake and infiltration. The soil moisture measured by the 5TE sensor in pits was in the range of 0.05–0.19. As such, the soil moisture content has a minor impact on the soil electrical conductivity as compared to the soil salinity.

To put the modeled true electrical conductivity σ into an agronomic sense, a relationship is needed to relate σ to soil salinity. A site specific petrophysical relationship is preferred as it can avoid errors arising from more general petrophysical schemes. To do this, sixteen soil samples were taken over a 0–80 cm depth to estimate the soil salinity. At each soil sample location, the σ_b was measured by inserting the 5TE sensor horizontally. In the laboratory, soil salinity was estimated by using the method of saturated soil-paste electrical conductivity [*Rhoades et al*., 1989]. First, distilled water was added to the air dried soil sample (200 g) and stirred to prepare saturated soil-paste. A stage is reached when all the pores in the soil are filled with water and the soil paste glistens as it reflects lights, flows slightly when the paste sample is tipped, and slides cleanly and freely off a spatula. The electrical conductivity of the soil paste sample EC_p was measured and a vacuum extraction procedure was used to remove the aqueous solution of the saturated paste. The electrical conductivity of the extracted solution was determined, and is usually referred to as the salinity of the saturated extract EC_e. As compared to other dilution/extraction methods, the saturation extract method minimizes the salt dissolution because less water is added [*Rhoades et al*., 1990].

2.5. Calibration of EMI Measurements

EMI measurements may have a static shift due to instrument calibration. For instance, *Lavoue et al*. [2010] observed a shift of 3–5 mS/m in EC_a after three repetitive EMI measurements along the same transect within 15 min intervals, with the only difference being recalibration of the system at the start of each profile measurement. They proposed a calibration procedure for EMI measurement by using a dipole-dipole configuration of electrical resistivity tomography (ERT) measurements. Calibration of EMI measurements is important when it comes to the quantitative interpretation of electrical conductivity values. In this paper, we used the vertical σ_b profile recorded in ten pits along the first transect of EMI measurement as an input for an electromagnetic forward model to generate the reference apparent electrical conductivity (EC_a^{ref}). The values of EC_a^{ref} were interpolated along the profile to provide more detailed information on lateral variations of electrical conductivity along the EMI transect and to compare with measured apparent electrical conductivity (EC_a^{meas}) by the CMD Mini-Explorer. Calibrated apparent electrical conductivity (EC_a^{cal}) was obtained by plotting a linear regressions between EC_a^{meas} and ECa_a^{ref} for each coil orientation. In order to evaluate the difference between measured and calculated data, the relative root mean square error (rRMSE) is formulated as follows:

$$rRMSE = 100 \times \sqrt{\frac{1}{M}\sum_{i=1}^{M}\left[\frac{EC_a^{ref}(i) - EC_a^{*}(i)}{EC_a^{ref}(i)}\right]^2} \tag{6}$$

where M is the number of measurements and $EC_a^{*}(i)$ is the value of measured or calibrated apparent electrical conductivity value. *Moghadas et al*. [2012] used a similar approach to calibrate EM38 and GSSI-profiler

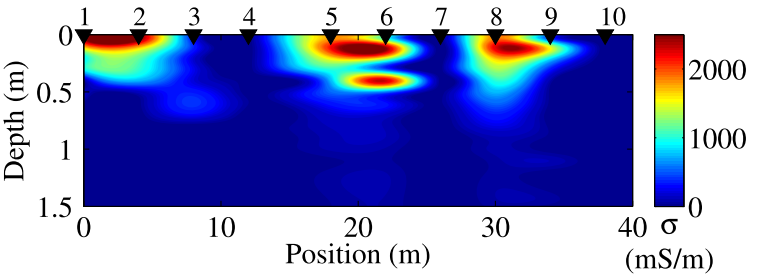

Figure 3. Plot of electrical conductivity (mS/m) measured by the 5TE capacitance sensors from 10 soil pits along transect 1. The black triangles indicate the location of the soil pits along the transect (Figure 2c).

measurements in the field by measuring the electrical conductivity of the soil cores taken along the EMI transect.

3. Results and Discussion

3.1. Ground-Truth Measurements

The bulk electrical conductivity of the soil, measured in each of the ten pits as a function of depth by the 5TE sensors, is presented in Figure 3. The black triangles correspond to the location of pits along this transect (see Figure 2 (c)). The two dimensional (2-D) profile of σ_b was constructed by using a cubic interpolation of the 150 capacitance sensor measurements. As can be seen, the infiltration front was recorded in each pit, with the infiltration bulb mostly contained within the top 50 cm of depth. High soil salinity and infiltration patterns at three different locations can be clearly identified. As discussed earlier, the EC_a is affected by the soil as a result of salt accumulation in the top soil due to the evaporation process. Field observation confirmed the salt accumulation, as in all pits salt crystals were observed in the top soil. The measured vertical profile of σ_b in each pit was used in the forward electromagnetic model to calculate EC_{ref} for calibration of the measured EMI data of that location. We compared 5TE electrical conductivity values measured using a frequency of 70 MHz with EMI data measured at 30 kHz. Electrical conductivity of soils with water content of 10% to 30% is frequency independent in the range of 0.5 kHz–5 MHz [*Delfino et al.*, 2009]. Therefore, our approach assumes a frequency independent of soil electrical conductivity for EMI and capacitance sensors.

Figure 4a show the relationship between the bulk electrical conductivity measured by using the 5TE sensor and the soil salinity at the same depth. The method used to measure the soil salinity is based on the electrical conductivity of a saturated soil-paste extract as described earlier. The red and black circles represent a single soil sample data collected between 0–10 cm and 10–80 cm depth, respectively. The black circles were used to plot a linear regression line between the measured σ_b and EC_e, which returns a coefficient of

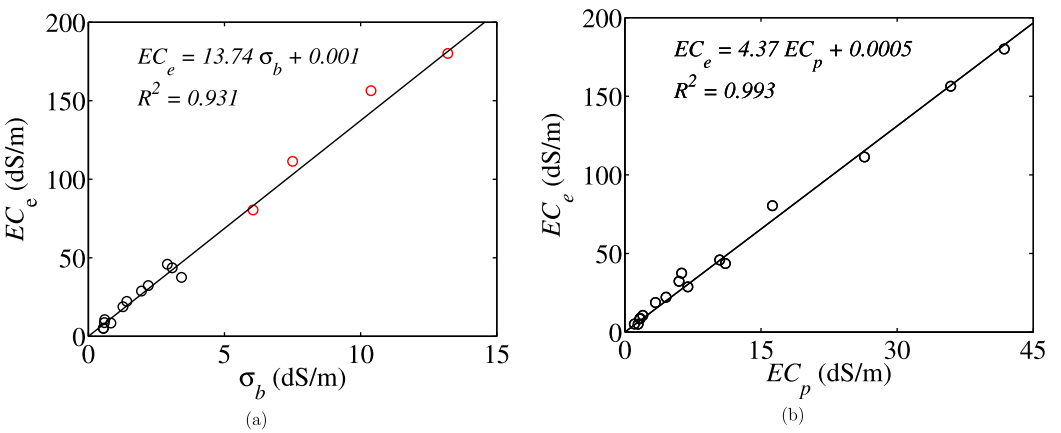

Figure 4. (a) Relationship between the bulk electrical conductivity (σ_b) and electrical conductivity of the saturated-paste extract (EC_e) measured for soil samples collected at different depths, red circles show data of soil samples collected in top 10 cm, which were not used to develop the linear regression. (b) relationship between the electrical conductivity of soil paste (EC_p) and EC_e.

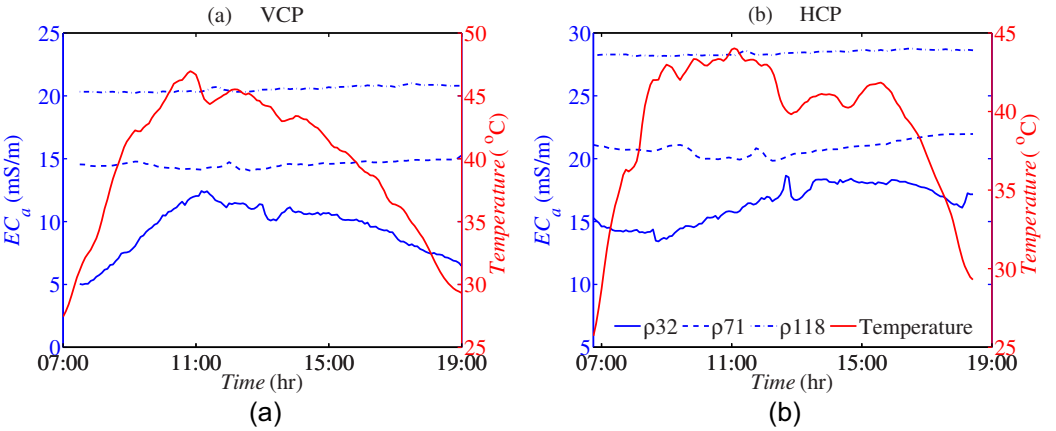

Figure 5. Change in ambient air temperature (red line) and the measured EC_a by three receivers at a spacing of 0.32, 0.71, 1.18 m from the transmitter, referred to here as ρ32, ρ71 and ρ118, (a) in vertical coplanar mode (VCP) and (b) in horizontal coplanar mode (HCP).

determination (R^2) value of 0.931. The measured EC_e and σ_b for the top soil sample between 0 and 10 cm fall along the regression line (shown by red circles), but were not used in developing the linear regression. The established linear relationship for a specific field [$EC_e = 13.74\ \sigma_b + 0.001$] was used to convert modeled σ by joint inversion of EMI measurements to EC_e profiles.

Figure 4b shows the plot between EC_e and EC_p. A typical linear relationship can be observed between EC_e and EC_p. The circle represent data obtained using a single soil sample that was extracted and diluted successively, as explained earlier. A linear regression line is plotted between EC_e and EC_p, which returns a R^2 value of 0.993 with a relationship of $EC_e = 4.37EC_p + 0.0005$ (see Figure 4b). The relation approaches to 0.0005 intercept point at zero salinity, which demonstrate the utility of the saturated soil-paste extract technique to measure precisely the salinity of the saturated extract EC_e. The intercept at zero salinity corresponds to the surface conductivity, which does not depend upon the salinity of the soil solution and upon the water content. Furthermore, *Rhoades et al.* [1990] reported that the conductivity of course dry soil is 0.000589 dS/m, which is close to what we have observed in our laboratory experiment results.

3.2. Temperature Stability of CMD Mini-Explorer

A fixed point drift experiment was conducted over a bare soil using the CMD Mini-Explorer to measure EC_a. During measurements, ambient air temperature increased from 26 to 46°C over the approximately 12 h period. Figures 5a and 5b show the ambient temperature and EC_a measured on consecutive days for VCP and HCP configuration over time. The instrument was given 1 h to equilibrate with the outdoor ambient temperature before starting measurements. Ambient temperature was recorded at 15 min intervals and the instrument was set up in a continuous measurement mode, with a time step of 20 s. Measured EC_a values were very stable for receivers spaced at ρ71 and ρ118 during the measurement time period of the VCP and HCP configuration (Figures 5a and 5b). Drift in the EC_a measurement for the ρ71 and ρ118 is minor and within the dynamic error range of the instrument ($<\pm$ 2mS/m per 20°C). At high temperatures, stability to the EC_a measurement is due to the internal calibration procedure adopted by the manufacturer [*GF-Instruments*, 2011]. The EC_a response for the ρ32 spacing showed a maximum fluctuation of 5 mS/m for the VCP and HCP configurations. The cause of this drift comes primarily from the sensitivity of the ρ32 to the soil moisture and soil temperature changes at shallow depth (0–50 cm). Overall the drift in the measurement of EC_a for all six configurations is negligible in the high temperature conditions of the study environment.

The measurement of EC_a with the CMD Mini-Explorer is very stable at high temperature as compared to other instruments previously used in the field. For instance, the Geonics EM38 system has been used extensively in the last three decades and *Robinson et al.* [2004] showed that when the internal temperature of the EM38 rises above 40°C, the instrument provides unexpected responses, with the EC_a increasingly underestimated. Furthermore, they reported that such drift is caused by a combination of placement of temperature compensation sensors and instrument factors that come down to circuit design and soil performance under heating. Furthermore, *Sudduth et al.* [2001] used a fixed point drift experiment for EM38 while the ambient temperature increased

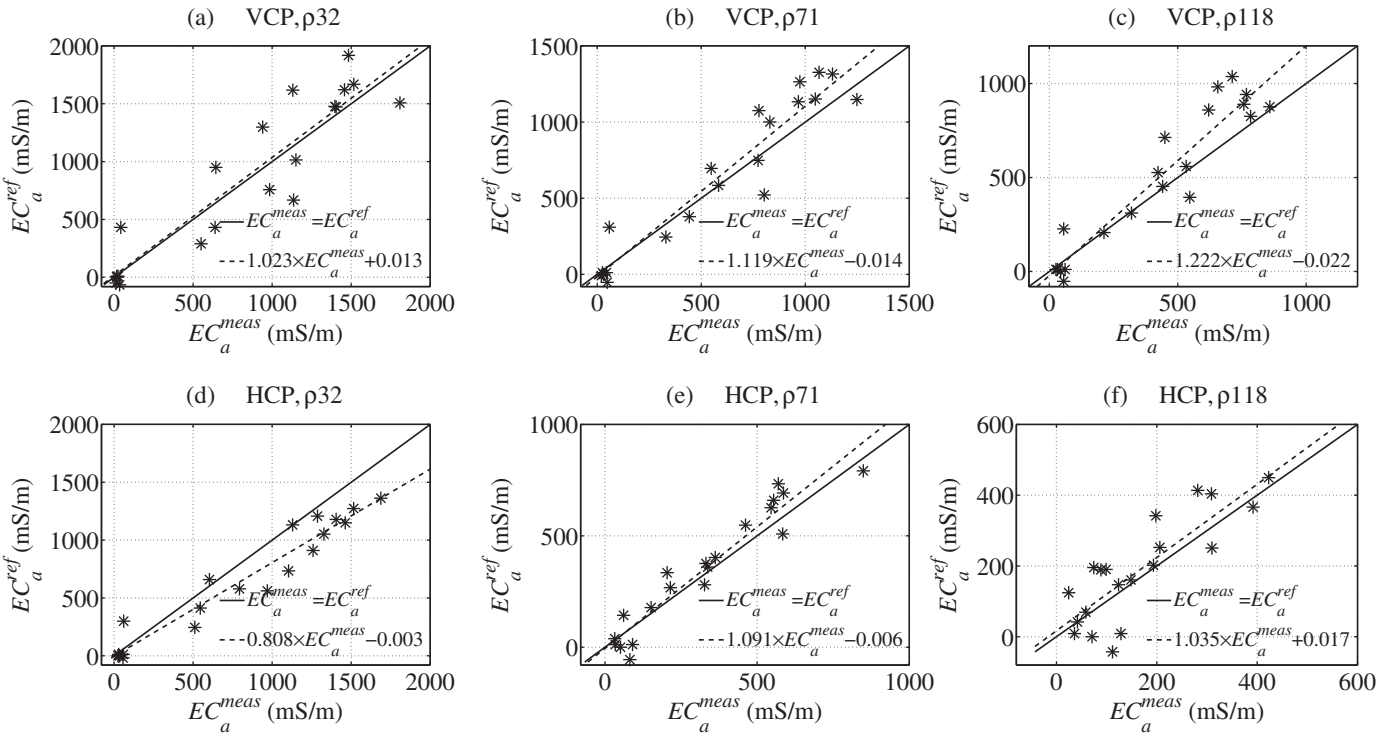

Figure 6. Scatter plots of measured (σ_a^{meas}) versus reference (σ_a^{ref}) apparent electrical conductivity for VCP and HCP modes using different instrument inter-coil spacing. Dashed lines present the corresponding linear regressions.

from 23 to 35°C over an 8 h period and EC_a increased from 32.2 to 42.3 mS/m, which represents a more than 25% drift. In such cases, temperature correction is applied using in situ measurement of vertical temperature profile within 1 meter depth to standardize field measured EC_a values by conversion to an equivalent electrical conductivity at a reference temperature of 25°C. As the CMD Mini-Explorer measurements are stable at high temperature there was no need to measure the vertical temperature profile in a pit for temperature correction. The DUALEM-1S system is less temperature sensitive compared to EM38-DD, with a maximum drift of 5.0 % (5.7 mS/m) observed [*Abdu et al.*, 2007].

3.3. Calibration and Inversion Results

Figure 6 shows a scatter plot of measured and reference apparent electrical conductivity in HCP and VCP configuration with different offsets. The right column shows the HCP mode and the left column shows the VCP mode with increasing coil spacings, ρ32, ρ71 and ρ118, from top to bottom. In all cases, the HCP and VCP results do not match the 1:1 (black solid) line, indicating the need for calibration of EMI measurements. The deviation from the 1:1 line shows EC_a^{ref} values are mostly larger in comparison to the EC_a^{meas}, except the HCP ρ32 configuration. To remove the bias, a linear regression between the EC_a^{meas} and EC_a^{ref} was derived from each scatter plot in Figure 6, with the resulting regression lines shown with dashed lines. The obtained regression parameters for the EC_a^{cal} are provided in the legends of Figure 6, which indicates that to remove the bias from the EC_a^{meas} each coil orientation requires a specific configuration. To investigate the bias, Table 1 presents the rRMSE between uncalibrated ($EC_a^{meas}-EC_a^{ref}$) and calibrated ($EC_a^{cal}-EC_a^{ref}$) data. The

Table 1. rRMSE Between Measured and Calculated Apparent Electrical Conductivity Values

Mode	Offset (m)	rRMSE Between Reference and Measured Values (%)	rRMSE Between Calibrated and Reference Values (%)
VCP	0.32	5.4	5.4
VCP	0.71	4.5	4.0
VCP	1.18	5.6	4.3
HCP	0.32	6.3	3.4
HCP	0.71	4.2	3.9
HCP	1.18	7.9	7.6

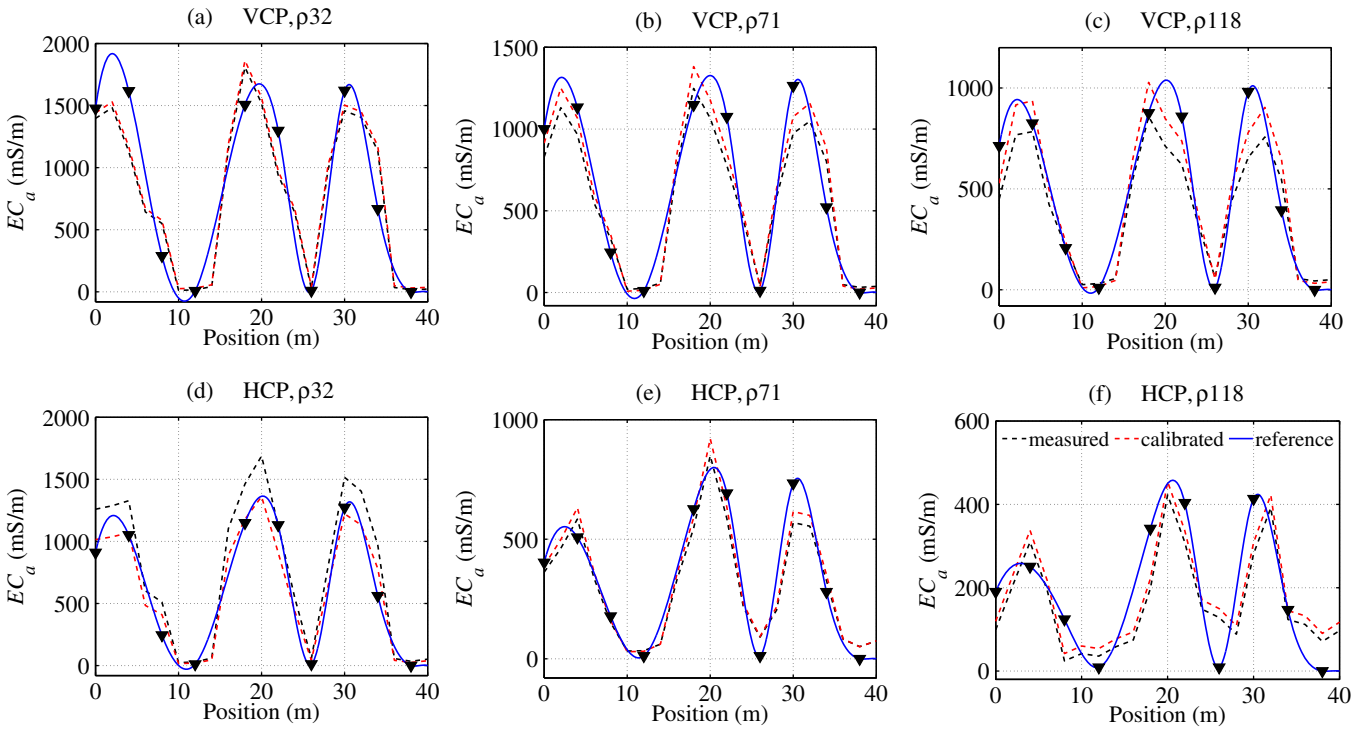

Figure 7. Reference (blue lines), measured (black dashed lines) and calibrated (red dashed lines) apparent electrical conductivity for vertical and horizontal dipole modes using different instrument offsets. The black triangles correspond to the location of the pits along the first EMI transect (Figure 2 c).

decrease in rRMSE due to the calibration can be observed. In particular, for the HCP ρ32 and VCP ρ118 configurations, the errors have been significantly reduced compared to the other configurations. These combined shift and scaling calibrations were applied to all the measured EC_a in the grid (see Figure 2c).

The measured, reference and calibrated apparent electrical conductivity values along the 40 m long transect are compared in Figure 7. The black triangles correspond to the location of the pits along the EMI transect, which were used for calibration of EMI measurements. It is notable that the three peaks show the location where drippers are used to irrigate the Acacia trees with brackish water (Figure 2c). The electrical conductivity decreases with depth as the salt concentration and soil moisture reduces with depth. As discussed earlier, soil moisture has less of an impact on the EC_a measurements as compared to the soil salinity. As a result, apparent electrical conductivity measured for all VCP configurations are higher than HCP, because VCP is sensitive to the shallow depth.

Figure 8 depicts the depth section of estimated soil electrical conductivity obtained from the joint inversion of multiconfiguration EC_a^{cal} measurements along the first transect. In total, 21

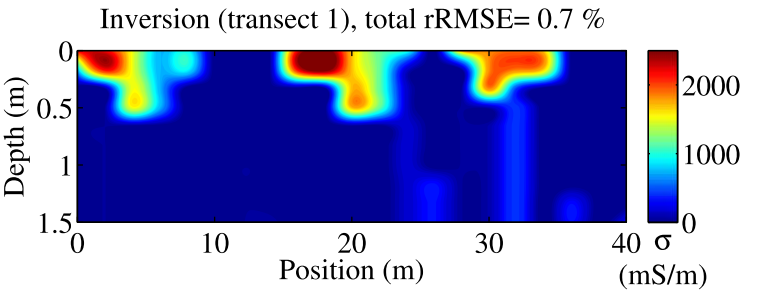

Figure 8. The depth profile of soil electrical conductivity obtained by using joint inversion of multiconfiguration EMI data for the first EMI transect.

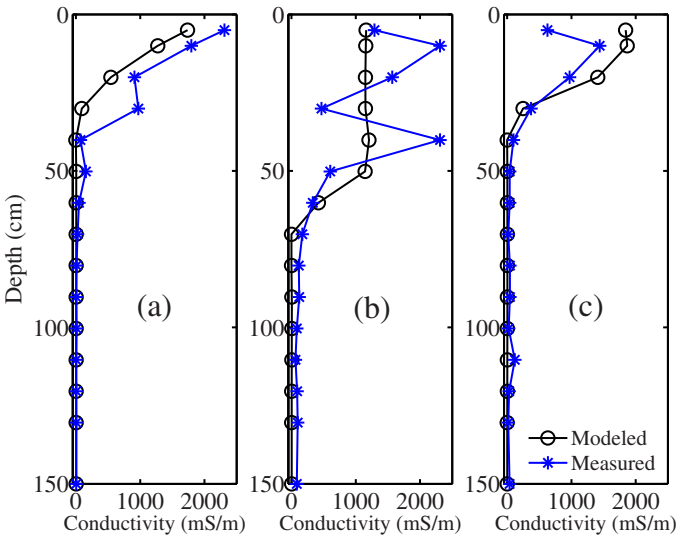

Figure 9. (a–c) The profile of the modeled true electrical conductivity (σ) from joint inversion of multiconfiguration of CMD Mini-Explorer (EC_a^{cal}) measurements and the bulk electrical conductivity (σ_b) measured using a capacitance sensor 5TE in three pits numbered as 1, 6, and 9 (Figure 2c), respectively.

multiconfiguration EC_a^{cal} measurements were inverted for a two-layer medium and later interpolated by using cubic convolution to obtain the vertical section of true modeled conductivity σ. For all inversions, the optimization parameter space was set relatively large, covering the whole range of values used for low and high electrical conductivity of soil; namely, $0 < \sigma_1 < 3000$ mS/m, $0 < \sigma_2 < 3000$ mS/m, and $0.01 < h_1 < 1.5$ m. The stopping criterion for the inversion was specified with respect to the convergence criterion in which an optimum was assumed to be reached when the objective function did not improve by more than 0.01% in 20 successive evolution loops. The soil salinity and the effect of infiltration patterns due to the drip irrigation can also be observed in the 2-D electrical conductivity plot obtained by EMI inversion. Inversion of multiconfiguration EC_a^{cal} data shows that the main structures and quantitative soil electrical conductivity values can be obtained and are in a good agreement with those derived by pit-based sensor measurements (Figure 3). Moreover, in the 2-D depth section of the soil electrical conductivity obtained by in situ 5TE measurements (Figure 3) or EMI inversion (Figure 8), it is difficult to discriminate the relative contributions of soil salinity, soil heterogeneity (e.g., texture) and soil moisture content. To reduce the effect of soil moisture, EMI and 5TE measurements were performed 8 h after the drip irrigation system was stopped. The soil salinity dominates other factors (i.e., soil moisture or soil texture), which effects EC_a measurements. As such, a field specific relationship was established between the soil electrical conductivity and soil salinity.

Figures 9a–9c present depth against modeled σ obtained from the joint inversion of multiconfiguration EC_a^{cal} measurements and the measured vertical profile of σ_b from the 5TE sensors in three pits: numbered 1, 6, and 9 (see Figure 2c). The profile of modeled σ was chosen from the interpolated 2D depth section of σ obtained in Figure 8, exactly at the 15 depths where σ_b were measured in the pits. In Figure 9, three different trends of σ_b can be observed in the top 50 cm depth. In pit 1, a decreasing trend from high to low values of σ_b was found. Fluctuating conductivity trends were measured in pit 6 with low σ_b in the top few cm, while a high to low conductivity trend was observed in pit 9. In all of the three trends of σ, the intersection between the high and low conductivity at a depth of 50 cm was well estimated from EMI measurements. The subsurface model was considered as a two layer medium for the joint inversion of multicomponent EMI measurements, so the trend of the conductivity variations in the top 50 cm of pits 6 and 9 were not well retrieved in modeled σ (Figures 9b and 9c). Complex distribution patterns of soil salinity and brackish water from a dripper, soil heterogeneity, and different sensing depth of sensors may cause the observed discrepancies. Comprehensive studies are required to investigate the uncertainty for multilayer earth models in a joint inversion scheme. Time-lapse EMI measurements can be performed to investigate the dynamics of the soil electrical conductivity and relate these to the soil salinity and water content distributions patterns [*Robinson et al.*, 2009; *Franz et al.*, 2011].

Figure 10 shows the response surfaces of the objective functions (station 17 of the first EMI transect) for the $\sigma_1-\sigma_2$, σ_1-h_1 and σ_2-h_1 parameter planes. The range of each parameter has been divided into 100 discrete values resulting in 10,000 objective function calculations for each plot. The white star

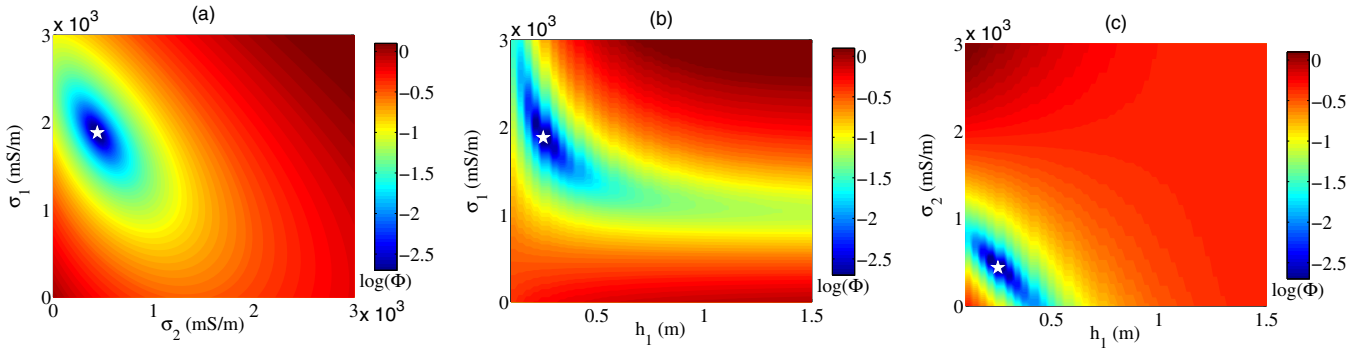

Figure 10. Response surfaces of the objective function (station 17 of the first EMI transect) in different parameter planes. The white star represents the values obtained by the joint inversion.

marker represents the inversely estimated parameters by the GMCS-NMS optimization algorithm. Response surface analysis of the objective function is important as it provides valuable insight into the uniqueness of the inverse solution and the sensitivity of the model to the different parameters, as well as any parameter correlations [*Moghadas et al.*, 2013]. Each surface shows a well-defined global minimum, partially illustrating the uniqueness of the solution for the given experimental design. In Figure 10, all the response surface parameters are negatively correlated to each other. The banana shaped contour plot in the $\sigma_1 - h_1$ space suggests negative correlation between these parameters, which is not informative for their estimation. The $\sigma_1 - \sigma_2$ and $\sigma_2 - h_1$ response surfaces exhibit a small elliptical shape showing negative correlation with a clear global minimum.

Figure 11 shows the spatial distribution of the calibrated apparent electrical conductivity for all HCP and VCP configurations. The patterns in σ_a are similar for all configurations, but the σ_a values of HCP are smaller than the VCP values. For example, the VCP $\rho 71$ measurements generally exceed 1,000 mS/m as compared

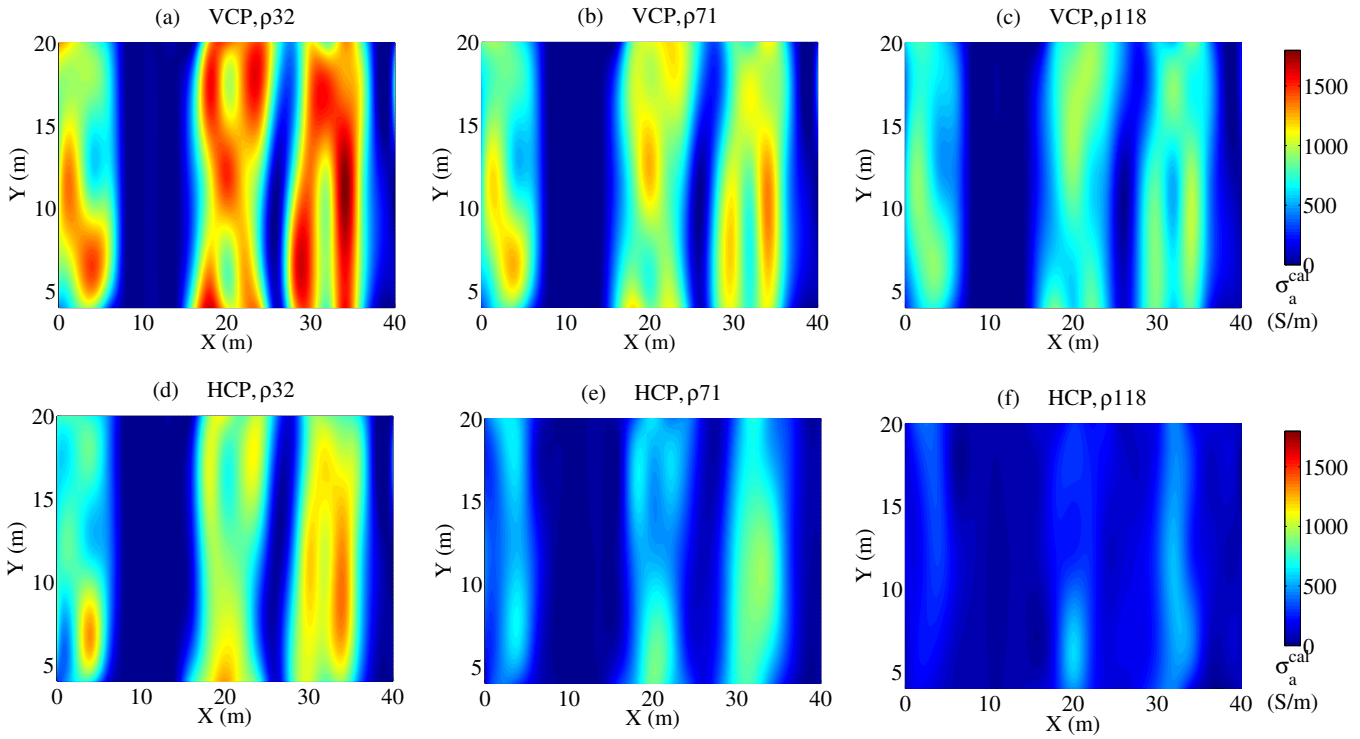

Figure 11. Maps of the calibrated apparent soil electrical conductivity for VCP and HCP configurations considering three different inter-coil spacing between transmitter and receiver.

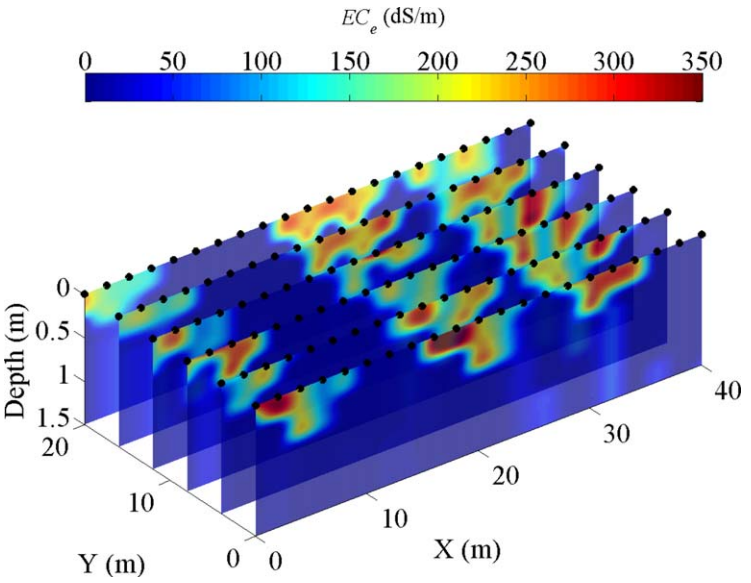

Figure 12. Spatial distribution of soil salinity (EC_e) obtained using joint inversion of multiconfiguration EMI measurements (calibrated EMI data) from the six transects. The black dots present the locations where the EMI measurements were performed.

with the HCP rho = 0.71 (m) measurements, which are smaller (i.e., < 1,000 mS/m). The VCP configuration having $\rho 32$ is sensitive to a 0.25 m depth and gives the largest σ_a (>1500 mS/m). Furthermore, EMI measurements using the HCP mode with 1.18 m inter-coil spacing presents $\sigma_a < 750$ mS/m. Since this configuration corresponds to 1.8 m effective penetration depth, it indicates that the brackish water did not infiltrate to a greater depth.

Figure 12 shows the spatial distribution of soil salinity derived from the estimated σ of six transects of EMI measurement. The soil salinity EC_e was estimated using the linear relationship established between $\sigma_b - EC_e$ measurements (Figure 4a). As noted earlier, the brackish water used to irrigate the Acacia trees was very saline, having high electrical conductivity (4200 mS/m). The effect of the brackish water infiltration from the drip irrigation system can be observed in the map of soil salinity obtained from the EMI data, with the three rows of high soil salinity indicating both the location of Acacia trees and also the infiltration front of the brackish water. The soil salinity and infiltration front ranges from 0.01 to 0.5 m depth. Results indicate that the quantitative analysis of the joint inversion of multiconfiguration EMI measurement using a full solution of Maxwell's equation permits the estimation of soil salinity caused by the brackish water infiltration. In the field Acacia threes roots were concentrated in the top 70 cm of soil and the low soil salinity below 30 cm (in Figure 12) shows that Acacia is capable of extracting salt solutions and reduces subsoil salinity. The results of this study provide detailed knowledge of the distribution pattern of soil salinity along different Acacia trees. In a next step time-lapse EMI measurements can be performed for better soil and water management practices.

4. Conclusions

Ground-based EMI methods can be used to determine boundaries of soil salinization in irrigated agricultural land. We investigated the ability of a new electromagnetic system, the CMD Mini-Explorer, to estimate soil salinity in a drip irrigation system using joint inversion of multiconfiguration EMI data. A field experiment was conducted in a farm where Acacia trees were irrigated with brackish water. Inversion results show that the depth of the infiltration front was well retrieved by considering a two-layer subsurface model. Differences were observed between the vertical bulk electrical conductivity profile measured with 5TE sensor and modeled electrical conductivity by EMI inversion. Discrepancies may originate from different sensing depth of sensors, soil heterogeneity, and complex distribution pattern of brackish water from drippers. The CMD Mini-Explorer readings over time were quite stable and the probe was less temperature sensitive and did not require field-specific temperature correction.

The tested approach enables the quantitative mapping of spatial electrical conductivity variations and can be used for soil salinity management. Moreover, joint inversion results provide conductivity variations with respect to the depth, which offers additional information as compared to traditional apparent conductivity imaging. Further research is needed to investigate the uncertainty resulting from different sources in the joint inversion: namely, pure measurement error (e.g., instrumental calibration and human error) and the modeling error (e.g., introduced by the petrophysical relationship and due to deficits in the electromagnetic model).

Acknowledgments

This work was supported by the Water Desalination and Reuse Center, King Abdullah University of Science and Technology (KAUST), Saudi Arabia. This project was initiated during a 3 month internship of Aurangzeb Jadoon at the Water Desalination and Reuse Center, KAUST. Data used in this paper can be made available on request. The authors are grateful to the local farmer Khadr Bin Sayed AlGamdi for his hospitality and providing access to his agricultural farm. John Triantafilis is acknowledged for his useful advice and many valuable suggestions. The authors are grateful to the Associate Editor Binayak Mohanty, Mark Everett, André *Revil*, and an anonymous reviewer for their constructive comments in improving the manuscript.

References

Abdu, H., D. Robinson, and S. Jones (2007), Comparing bulk soil electrical conductivity determination using the dualem-1s and EM38-DD electromagnetic induction instruments, *Soil Sci. Soc. Am. J.*, *71*(1), 189–196.

Adamchuk, V. I., J. W. Hummel, M. T. Morgan, and S. K. Upadhyaya (2004), On-the-go soil sensors for precision agriculture, *Comput. Electronics Agric.*, *44*(1), 71–91.

Allbed, A., and L. Kumar (2013), Soil salinity mapping and monitoring in arid and semi-arid regions using remote sensing technology: A review, *Adv. Remote Sens.*, *2*(4), 373–385.

Anderson, W. L. (1979), Numerical integration of related hankel transforms of orders 0 and by adaptive digital filtering, *Geophysics*, *44*(7), 1287–1305.

Bonsall, J., R. Fry, C. Gaffney, I. Armit, A. Beck, and V. Gaffney (2013), Assessment of the CMD Mini-Explorer, a new low-frequency multi-coil electromagnetic device, for archaeological investigations, *Archaeological Prospect.*, *20*(3), 219–231.

Borchers, B., T. Uram, and J. M. H. Hendrickx (1997), Tikhonov regularization of electrical conductivity depth profiles in field soils, *Soil Sci. Soc. Am. J.*, *61*(4), 1004–1009.

Borner, F. (2006), *Complex Conductivity Measurements, Groundwater Geophysics, a Tool for Hydrogeology*, pp. 119–153, Springer, Berlin.

Bower, C. A., and L. V. Wilcox (1965), *Methods of Soils Analysis*, vol. 2, Am. Soc. of Agron., Madison.

Callegary, J. B., T. P. A. Ferre, and R. W. Groom (2007), Vertical spatial sensitivity and exploration depth of low-induction-number electromagnetic-induction instruments, *Vadose Zone J.*, *6*(1), 158–167.

Corwin, D. L., and S. M. Lesch (2005a), Characterizing soil spatial variability with apparent soil electrical conductivity: Part II. Case study, *Comput. Electronics Agric.*, *46*(1-3), 135–152.

Corwin, D. L., and S. M. Lesch (2005b), Apparent soil electrical conductivity measurements in agriculture, *Comput. Electronics Agric.*, *46*(1-3), 11–43.

Corwin, D. L., S. M. Lesch, J. D. Oster, and S. R. Kaffka (2006), Monitoring management-induced spatio-temporal changes in soil quality through soil sampling directed by apparent electrical conductivity, *Geoderma*, *131*(3-4), 369–387.

Craig, G. F., C. A. Atkins, and D. T. Bell (1991), Effect of salinity on growth of 4 strains of rhizobium and their infectivity and effectiveness on 2 species of acacia, *Plant Soil*, *133*(2), 253–262.

Delfino, F., R. Procopio, M. Rossi, and F. Rachidi (2009), Influence of frequency-dependent soil electrical parameters on the evaluation of lightning electromagnetic fields in air and underground, *J. Geophys. Res.*, *114*, D11113, doi:10.1029/2008JD011127.

Ershadi, A., M. F. McCabe, J. P. Evans, N. W. Chaney, and E. F. Wood (2014), Multi-site evaluation of terrestrial evaporation models using fluxnet data, *Agric. For. Meteorol.*, *187*, 46–61.

Everett, M. E. (2012), Theoretical developments in electromagnetic induction geophysics with selected applications in the near surface, *Surv. Geophys.*, *33*(1), 29–63.

Franz, T. E., E. G. King, K. K. Caylor, and D. A. Robinson (2011), Coupling vegetation organization patterns to soil resource heterogeneity in a central Kenyan dryland using geophysical imagery, *Water Resour. Res.*, *47*, W07531, doi:10.1029/2010WR010127.

Fritz, R. M., D. D. Malo, T. E. Schumacher, D. E. Clay, C. G. Carlson, M. M. Ellsbury, and K. J. Dalsted (1999), Field comparison of two soil electrical conductivity measurement systems, in *Proceedings of the Fourth International Conference on Precision Agriculture*, Parts A and B, edited by P. C. Robert, R. H. Rust, and W. E. Larson, pp. 1211–1217, Am. Soc. of Agron., Madison.

Ganjegunte, G. K., Z. Sheng, and J. A. Clark (2014), Soil salinity and sodicity appraisal by electromagnetic induction in soils irrigated to grow cotton, *Land Degrad. Dev.*, *25*(3), 228–235.

GF-Instruments (2011), *CMD Electromagnetic Conductivity Meter User Manual v. 1.5*, Geophys. Equip. and Serv.

Huyer, W., and A. Neumaier (1999), Global optimization by multilevel coordinate search, *J. Global Optim.*, *14*(4), 331–355.

Jadoon, K. Z., S. Lambot, E. C. Slob, and H. Vereecken (2011), Analysis of horn antenna transfer functions and phase-center position for modeling off-ground GPR, *IEEE Trans. Geosci. Remote Sens.*, *49*(5), 1649–1662.

Jardani, A., A. Revil, F. Santos, C. Fauchard, and J. P. Dupont (2007), Detection of preferential infiltration pathways in sinkholes using joint inversion of self-potential and EM-34 conductivity data, *Geophys. Prospect.*, *55*(5), 749–760.

Keller, G., and F. Frischknecht (1966), *Electrical Methods in Geophysical Prospecting, int. Ser. Monogr. Electromagn. Waves 10*, Pergamon, Oxford, U. K.

Lagarias, J. C., J. A. Reeds, M. H. Wright, and P. E. Wright (1998), Convergence properties of the nelder-mead simplex method in low dimensions, *SIAM J. Optim.*, *9*(1), 112–147.

Lavoue, F., J. van der Kruk, J. Rings, F. Andre, D. Moghadas, J. A. Huisman, S. Lambot, L. Weihermuller, J. Vanderborght, and H. Vereecken (2010), Electromagnetic induction calibration using apparent electrical conductivity modelling based on electrical resistivity tomography, *Near Surf. Geophys.*, *8*(6), 553–561.

Lesch, S. M., D. J. Strauss, and J. D. Rhoades (1995), Spatial prediction of soil salinity using electromagnetic induction techniques: 1. statistical prediction models: A comparison of multiple linear regression and cokriging, *Water Resour. Res.*, *31*(2), 373–386.

Li, H. Y., Z. Shi, R. Webster, and J. Triantafilis (2013), Mapping the three-dimensional variation of soil salinity in a rice-paddy soil, *Geoderma*, *195*, 31–41.

McNeill, J. D. (1980), Electromagnetic terrain conductivity measurement at low induction numbers, *Tech. Note TN-6*, Geonics Ltd., Mississauga, Ont., Canada.

Mester, A., J. van der Kruk, E. Zimmermann, and H. Vereecken (2011), Quantitative two-layer conductivity inversion of multi-configuration electromagnetic induction measurements, *Vadose Zone J.*, *10*(4), 1319–1330.

Minsley, B. J. (2011), A trans-dimensional bayesian markov chain monte carlo algorithm for model assessment using frequency-domain electromagnetic data, *Geophys. J. Int.*, *187*(1), 252–272.

Moghadas, D., F. Andre, E. C. Slob, H. Vereecken, and S. Lambot (2010), Joint full-waveform analysis of off-ground zero-offset ground penetrating radar and electromagnetic induction synthetic data for estimating soil electrical properties, *Geophys. J. Int.*, *182*(3), 1267–1278.

Moghadas, D., F. Andre, J. H. Bradford, J. van der Kruk, H. Vereecken, and S. Lambot (2012), Electromagnetic induction antenna modelling using a linear system of complex antenna transfer functions, *Near Surf. Geophys.*, *10*(3), 237–247.

Moghadas, D., K. Z. Jadoon, J. Vanderborght, S. Lambot, and H. Vereecken (2013), Effects of near surface soil moisture profiles during evaporation on far-field ground-penetrating radar data: A numerical study, *Vadose Zone J.*, *12*(2), doi:10.2136/vzj2012.0138.

Revil, A. (2012), Spectral induced polarization of shaly sands: Influence of the electrical double layer, *Water Resour. Res.*, *48*, W02517, doi: 10.1029/2011WR011260.

Revil, A., P. Kessouri, and C. Torres-Verdín (2014), Electrical conductivity, induced polarization, and permeability of the fontainebleau sandstone, *Geophysics*, *79*(5), D301–D318.

Rhoades, J. D., P. A. C. Raats, and R. J. Prather (1976), Effects of liquid-phase electrical conductivity, water content, and surface conductivity on bulk soil electrical conductivity, *Soil Sci. Soc. Am. J.*, *40*(5), 651–655.

Rhoades, J. D., N. A. Manteghi, P. J. Shouse, and W. J. Alves (1989), Estimating soil-salinity from saturated soil-paste electrical-conductivity, *Soil Sci. Soc. Am. J.*, *53*(2), 428–433.

Rhoades, J. D., P. J. Shouse, W. J. Alves, N. A. Manteghi, and S. M. Lesch (1990), Determining soil salinity from soil electrical conductivity using different models and estimates, *Soil Sci. Soc. Am. J.*, *54*, 46–54.

Rhoades, J. D., F. Chanduvi, and S. M. Lesch (1999), Soil salinity assessment: Methods and interpretation of electrical conductivity measurements, *FAO Irrig. Drainage Pap.*, *57*, FAO, Rome.

Robinson, D. A., I. Lebron, S. M. Lesch, and P. Shouse (2004), Minimizing drift in electrical conductivity measurements in high temperature environments using the EM-38, *Soil Sci. Soc. Am. J.*, *68*(2), 339–345.

Robinson, D. A., I. Lebron, B. Kocar, K. Phan, M. Sampson, N. Crook, and S. Fendorf (2009), Time-lapse geophysical imaging of soil moisture dynamics in tropical deltaic soils: An aid to interpreting hydrological and geochemical processes, *Water Resour. Res.*, *45*, W00D32, doi: 10.1029/2008WR006984.

Rudolph, S., J. van der Kruk, C. von Hebel, M. Ali, M. Herbst, C. Montzka, S. Patzold, D. A. Robinson, H. Vereecken, and L. Weihermuller (2015), Linking satellite derived lai patterns with subsoil heterogeneity using large-scale ground-based electromagnetic induction measurements, *Geoderma*, *241*, 262–271.

Santos, F. A. M. (2004), 1-D laterally constrained inversion of EM34 profiling data, *J.f Appl. Geophys.*, *56*(2), 123–134.

Santos, F. A. M., J. Triantafilis, R. S. Taylor, S. Holladay, and K. E. Bruzgulis (2010), Inversion of conductivity profiles from EM using full solution and a 1-D laterally constrained algorithm, *J. Environ. Eng. Geophys.*, *15*(3), 163–174.

Sudduth, K. A., S. T. Drummond, and N. R. Kitchen (2001), Accuracy issues in electromagnetic induction sensing of soil electrical conductivity for precision agriculture, *Comput. Electronics Agric.*, *31*, 239–264.

Sudduth, K. A., N. R. Kitchen, G. A. Bollero, D. G. Bullock, and W. J. Wiebold (2003), Comparison of electromagnetic induction and direct sensing of soil electrical conductivity, *Agron. J.*, *95*(3), 472–482.

Sudduth, K. A., N. R. Kitchen, W. J. Wiebold, W. D. Batchelor, G. A. Bollero, D. G. Bullock, D. E. Clay, H. L. Palm, F. J. Pierce, R. T. Schuler, and K. D. Thelen (2005), Relating apparent electrical conductivity to soil properties across the north-central USA, *Comput. Electronics Agric.*, *46*(1-3), 263–283.

Triantafilis, J., G. M. Laslett, and A. B. McBratney (2000), Calibrating an electromagnetic induction instrument to measure salinity in soil under irrigated cotton, *Soil Sci. Soc. Am. J.*, *64*(3), 1009–1017.

Veseyfitzgerald, D. F. (1957), The vegetation of the red sea coast north of Jedda, Saudi Arabia, *J. Ecol.*, *45*(2), 547–562.

von Hebel, C., S. Rudolph, A. Mester, J. A. Huisman, P. Kumbhar, H. Vereecken, and J. van der Kruk (2014), Three-dimensional imaging of subsurface structural patterns using quantitative large-scale multiconfiguration electromagnetic induction data, *Water Resour. Res.*, *50*, 2732–2748, doi:10.1002/2013WR014864.